Developing an Experimental Basis for Understanding Transport in NIF Hohlraum Plasmas

M. A. Barrios,[1,*] J. D. Moody,[2] L. J. Suter,[2] M. Sherlock,[2] H. Chen,[2] W. Farmer,[2] J. Jaquez,[3] O. Jones,[2] R. L. Kauffman,[2] J. D. Kilkenny,[2] J. Kroll,[2] O. L. Landen,[2] D. A. Liedahl,[2] S. A. Maclaren,[2] N. B. Meezan,[2] A. Nikroo,[2] M. B. Schneider,[2] D. B. Thorn,[2] K. Widmann,[2] and G. Pérez-Callejo[4]

[1]*In-Q-Tel, Menlo Park, California 94025, USA*

[2]*Lawrence Livermore National Laboratory, Livermore, California 94551, USA*

[3]*General Atomics, San Diego, California 92186, USA*

[4]*Department of Physics, Clarendon Laboratory, University of Oxford, Parks Road, Oxford OX1 3PU, United Kingdom*

(Received 21 January 2018; revised manuscript received 22 July 2018; published 31 August 2018)

We report on the first multilocation electron temperature (T_e) and flow measurements in an ignition hohlraum at the National Ignition Facility using the novel technique of mid-Z spectroscopic tracer "dots." The measurements define a low resolution "map" of hohlraum plasma conditions and provide a basis for the first multilocation tests of particle and energy transport physics in a laser-driven x-ray cavity. The data set is consistent with classical heat flow near the capsule but reduced heat flow near the laser entrance hole. We evaluate the role of kinetic effects, self-generated magnetic fields, and instabilities in causing spatially dependent heat transport in the hohlraum.

DOI: 10.1103/PhysRevLett.121.095002

At the conclusion of the National Ignition Campaign [1], a three-year project to demonstrate indirect drive ignition and gain at the National Ignition Facility (NIF), the implosion experiments had identified specific physics issues which, if overcome, could significantly increase the performance and gain [2]. The experiments showed reduced x-ray drive, greater laser attenuation, and significantly more laser-plasma instabilities than simulated [3]. Simulations of high energy density (HED) plasmas encountered in inertial confinement fusion or in astrophysics often use reduced physics models of heat transport, atomic emissivity, opacity, nonlocal thermal equilibrium, and self-generated magnetic fields. For example, heat flux is modeled as $q = \min(q_{\mathrm{SH}}, f q_{fs})$, where $q_{\mathrm{SH}} = \kappa_{\mathrm{SH}} \nabla T_e$ is the classical Spitzer-Harm (SH) heat flux and f is a flux-limiting multiplier to the free-streaming (maximum) heat flux $q_{fs} \sim n_e v_{te} \kappa_B T_e$ [4]. This approximates heat transport when the electron-ion mean-free-path λ_{ei} exceeds $\sim$1% of the temperature gradient $T_e/\|\nabla T_e\|$ and the classical description fails [5]. Highly averaged atomic models for calculating ionization balance provide results of comparable accuracy to detailed models but at much lower computational cost [6]. Magnetohydrodynamic (MHD) effects are generally modeled using a fluid expression of Ohm's law [7,8], but models which include both MHD and flux-limited heat transport are not readily available or tested. The lack of experimental data available for testing each of these reduced models presents a significant need in HED physics.

As a result, we undertook experiments to characterize the hohlraum plasma conditions (principally T_e) for the purpose of developing a more experimentally based understanding of hohlraum physics. The experimental strategy focused on creating a low-resolution spatial "map" of plasma conditions which would serve as a starting point for deconstructing the complex picture of transport in a NIF hohlraum. Multilocation T_e measurements in a plasma offer a more constrained and stronger test of the models than single location measurements.

Hohlraum temperature measurements are difficult due to limited access and high optical and x-ray background levels. Time-resolved T_e measurements at a single spatial location in a hohlraum have been successful when using either optical Thomson scattering (OTS) [9,10] or spectroscopic line emission [11,12]. A multilocation T_e measurement in a cylindrical cavity laser heated from one end was successfully demonstrated on the Omega laser [10,13] using imaging OTS. These data were important for quantifying thermal transport along the cavity axis. Based on readily available NIF x-ray spectrometers and specialized target fabrication capabilities as well as interest in accessing high-density regions near the capsule and Au wall, we decided to undertake the first T_e measurements in the NIF hohlraum using x-ray line emission spectroscopy.

In this Letter we report on the first multilocation temperature measurements in a NIF ignition target design using x-ray spectroscopy. The main results consist of T_e at three hohlraum locations with different transport physics. We find that the three temperature measurements are initially consistent with classical (SH) heat transport; later in time, the higher temperature region near the laser entrance hole (LEH) indicates reduced heat transport.

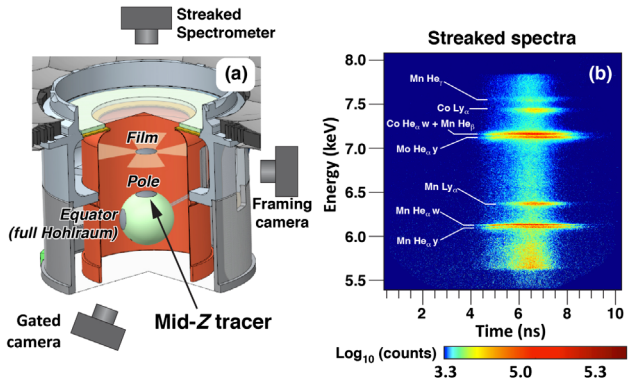

FIG. 1. (a) A sketch of the ViewFactor target used for two of the three starting locations of the mid-Z tracer dot. The equatorial dot is studied in a full-sized hohlraum. (b) The streaked spectral data for the dot on film experiment; the labels indicate Mn and Co w ($1s2p\ ^1P_1 - 1s^2\ ^1S_0$), y ($1s2p\ ^3P_1 - 1s^2\ ^1S_0$), and Ly$\alpha$ ($2p\ ^2P_{1/2,3/2} - 1s\ ^2S_{1/2}$) lines.

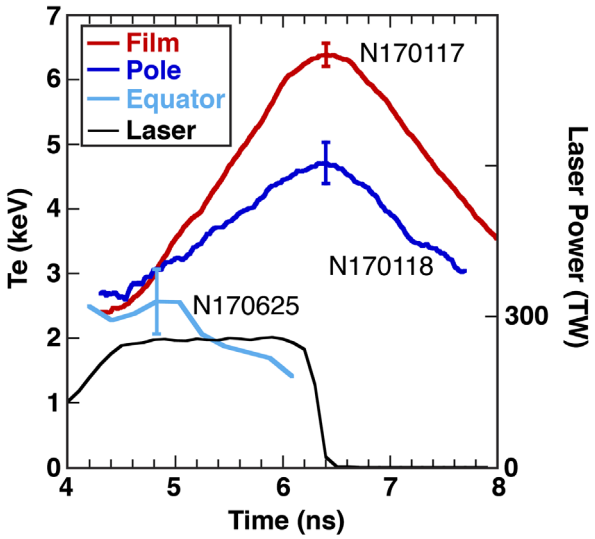

FIG. 2. Plot shows the time history of T_e for the dot on the film (red), the dot on the "north pole" of the capsule (dark blue) and the dot on the equator of the capsule (light blue). The laser power is plotted for the film and north-pole dots; the equatorial dot was in a full hohlraum and used 33% more laser power. The curves are labeled with the NIF shot numbers.

We discuss the role of kinetic effects (nonlocal transport [5]), laser-generated magnetic fields [7], and instabilities [14] in accounting for the observations.

Figure 1(a) shows a sketch of the gold (Au) "ViewFactor" hohlraum [15] used for measurements with the tracer on the film or pole. The hohlraum is 0.65 cm long, 0.5 cm diameter, cooled to 32 K, filled with 0.3 mg/cc of He, and uses a CH capsule with 1.5 mm inner radius and 0.03 mm thickness. Removal of the lower ~25% of the hohlraum minimizes the broadband Au background emission but still creates plasma conditions above a horizontal plane through the center of the capsule which are similar to the full ignition hohlraum [2]. The equatorial tracer was studied in a full hohlraum which used a 0.844 mm inner radius and 0.064 mm thick high-density carbon capsule. The Mn-Co tracer is sputter coated on the capsule pole [12] or the LEH side of an 0.5 μm thick CH film in the shape of an X suspended between the capsule and the LEH (3.175 ± 0.025 mm from the capsule center). The film sag is < 60 μm. The tracer is a solid disk of about 0.98 mm diameter and thickness of 0.165 ± 0.01 μm (pole) or 0.33 ± 0.02 μm (film). The Mn-Co tracer composition is equal parts Mn and Co (±5%). The equator tracer (Mn-only) is 0.4 mm diameter and 0.15 μm thick. Figure 1(b) shows data from the streaked spectrometer [12], and labels identify lines from the Mn-Co tracer materials used to estimate T_e [11,12,16,17].

The spectrometer is moved to the equatorial plane to measure emission from the equatorial tracer. Mn-line emission passes through the capsule and an 0.8 mm square by 80 μm thick diamond window on the hohlraum wall before reaching the spectrometer. The diamond window was positioned opposite the tracer so as not to perturb the plasma flow near the tracer.

The experiments are performed using a selection of the 192 NIF lasers [18]. The beams enter the target chamber in 2×2 groups called a quad; the quads are positioned in four separate cones on each of the northern and southern chamber hemispheres. The two inner cones are at 23.5° and 30° (3.4×10^{14} W/cm^2 quad intensity at best focus) and the two outer cones are at 44.5° and 50° (8.1×10^{14} W/cm^2 quad intensity at best focus) relative to the hohlraum axis. All quads reach best focus at the LEH. Measurements of backscatter show ≤4% stimulated Brillouin scattering at the end of the laser pulse. The 128 beams consisting of all upper hemisphere beams, and the inner cones on the lower hemisphere are used for the ViewFactor experiments, delivering a total of 0.7 MJ of laser energy and a peak laser power of 280 TW to the target. The full hohlraum target used 188 beams.

Figure 2 shows the $T_e(t)$ estimated from the Mn (and Co) lines for the three tracer locations. The laser pulse (black) is for the ViewFactor experiments; the full hohlraum pulse is scaled by 1.33×. Spectral data analysis uses SCRAM [19] to generate synthetic isothermal spectra and determines the sum of the squares of the residuals (data—model) on a two-axis grid of T_e and an anisotropy scale factor (ranging from 0.5 to 1.5 based on the experimental conditions) to accommodate the resonant absorption and reemission of the w lines [20,21]. The residuals show weak sensitivity to the electron density [for 0.2×10^{20} cm$^{-3} \lesssim n_e \lesssim 15 \times 10^{20}$ cm^{-3}] and little change with a two-temperature electron population. We determine the most probable $T_e(t)$ from the peak of the marginal probability distribution obtained by integrating over the anisotropy factor [22]. Figure 3 shows an example of the measured spectra for the three tracer locations at one point in time and the SCRAM fit

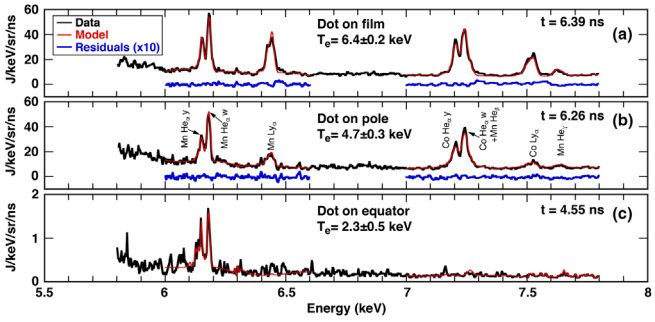

FIG. 3. The figures show the spectral data (black), the fit (red), and the residuals [(data—model)×10] in the main spectral line energy regions for (a) the dot on film, (b) the dot on the capsule, and (c) the equatorial dot (where the data-model difference is visible by inspection).

using the most probable T_e at the given time. The T_e error includes uncertainty in spectrometer calibration, tracer material stoichiometry, and the 95% confidence interval in the most likely T_e. The ionization time lag, which could give a lower T_e result, is negligible in simulations for the two capsule tracers but may be important for the film tracer due to the lower local electron density. We evaluated this by comparing the $T_e(t)$ from the full Mn-Co spectra with the $T_e(t)$ from only the Mn or the Co interstage lines (more sensitive to ionization lag). We find a similar $T_e(t)$ time history in this comparison indicating the ionization lag is within the uncertainty in T_e.

The tracer material is not stationary but expands and moves as lasers heat the hohlraum and cause ablation from the interior surfaces. We observe the tracer emission trajectory through a front vertical diamond window in the side of the hohlraum [see Fig. 1(a)]. Gated camera images taken from below the target show that the perturbation caused by the window plasma is limited to a region of ~250 μm surrounding the window [23].

Figure 4(a) shows the emission trajectory constructed from 16 time-spaced images for the pole and film tracers, and Fig. 4(b) shows 0.1 ns gated images of the tracer emission observed through the vertical window. The position uncertainty is ±100 μm. A separate rear window on the opposite hohlraum wall (~20% larger) minimizes Au background emission. Slight misalignment of the two windows produces emission visible along some of the window edges. The 80 μm thick window is sized to leave a 50 μm perimeter gap. Simulations show that this gap partially fills with carbon plasma which is more transmissive to the tracer emission. This allows brighter emission at the edges of the window that can be seen in the dot on film image. Side-view camera filtering [24] limits the x-ray emission reaching the detector to the 6–9 keV range emphasizing the Mn and Co line emission.

We modeled the experiment with the LASNEX [25] radiation hydrodynamic code using an adjustable flux limiter [4] applied throughout the hohlraum and an atomic configuration model called detailed configuration accounting (DCA) [6]; no MHD effects were included in these simulations. Insights into hohlraum physics come from noting where LASNEX shows good and poor agreement with the observations. For example, Fig. 4(c) shows that classical SH heat transport, obtained with $f = 0.15$, gives good agreement with the equatorial T_e throughout the experiment. Note that both the measured and simulated T_e start to decrease at $t = 5$ ns. The simulations show that this is caused by the Au-wall plasma generated by the outer laser beams starting to blow into the inner beam path and absorbing the inner beam power. The attenuation of the equatorial laser drive causes the T_e to fall. Indeed, recent measurements to quantify inner beam transport give support to this explanation [26].

The pole data in Fig. 4(d) are not fit well by either choice of f and suggest that a midrange flux limiter may be optimum. A restrictive flux limiter shows a good match with the film T_e in Fig. 4(e). This restricted heat flux may be due to nonlocal heat transport. Estimating the temperature gradient scale length at the end of peak power from

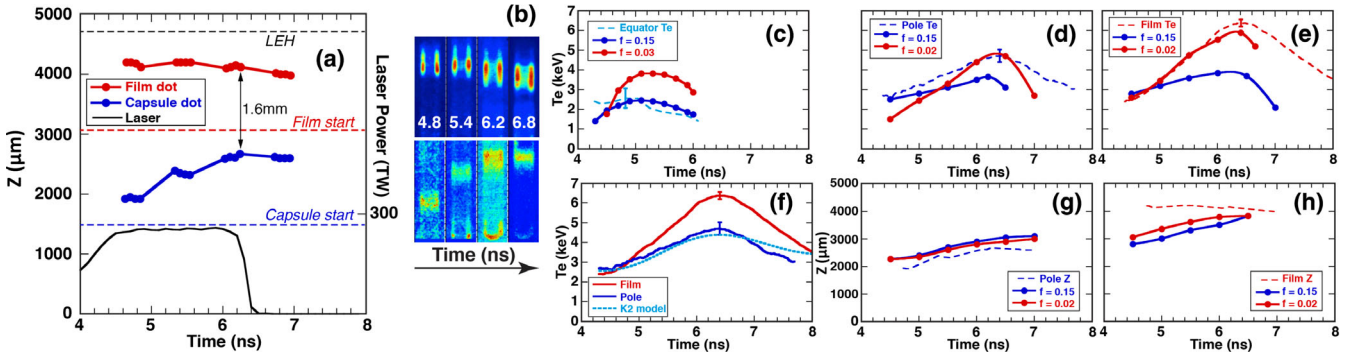

FIG. 4. (a) Tracer emission trajectories constructed from framing camera images of the Mn-Co emission. (b) Framing camera images show the time- and space-resolved tracer emission. Data (in dotted line) and the LASNEX-simulated temperature are shown for (c) the dot on the equator, (d) the dot on the pole, and (e) the dot on the film. The K2-simulated T_e for the pole using the film T_e as input is shown in (f). The LASNEX-simulated emission location is shown for the dot on the pole (g) and the dot on the film (h).

the pole and film tracers gives a temperature difference of ~1.7 keV over an axial distance of 1.6 mm for $L_T = T_e/(\partial T_e/\partial z)$ of ~5 mm. The electron-ion mean free path is $0.14\ \text{mm} \le \lambda_{ei} \le 1\ \text{mm}$, which gives $\lambda_{ei}/L_T \ge 0.03$ and satisfies the condition for nonlocal electron heat transport [5].

The question arises as to whether nonlocality alone can account for the observed persistence of a strong temperature gradient. To investigate this, we simulated the transport between the pole and film dots using the Fokker-Planck model K2 [14]. The density is fixed at $n_e = 2 \times 10^{20}\ \text{cm}^{-3}$, and the laser-heated plasma is assumed to be a sphere with radius ≈1 mm. This region, which represents the plasma surrounding the dot on film, is heated so its T_e follows the measurement. The temperature at a radius of 1.6 mm is monitored (representing the approximate location of the dot on the capsule). The results, plotted in Fig. 4(f), indicate that the observed delay in heating of the dot on capsule region can be reasonably well accounted for by nonlocal effects. In a SH model, the temperature of the dot on the capsule would closely follow that of the dot on the film.

We conclude that under simplified conditions, nonlocality can in principle account for the observations, but in reality it may play a complementary role and other contributing processes should be considered, most notably magnetic fields [7,8]. MHD simulations suggest the $\nabla n_e \times \nabla T_e$ mechanism will generate magnetic fields strong enough to inhibit heat flow between the dots. However, such simulations use local transport theory. The return current instability [27] is driven by strong temperature gradients, but for these conditions we find nonlocal effects are likely stabilizing. The growth rates for the thermomagnetic and collisional Weibel instabilities [28] are relatively small ($\lesssim 10^{-10}\ \text{s}^{-1}$) and therefore don't affect T_e gradients. These considerations highlight the importance of developing hohlraum transport models that simultaneously account for nonlocality and magnetization.

The simulated tracer emission trajectory shows significant differences relative to the data. For example, Fig. 4(g) shows an offset of +200 to +300 μm in the simulated pole emission position for either value of f; the simulated film emission in Fig. 4(h) starts 1 mm below the measurement and gradually approaches the measured location. There is evidence from the measured Mn and Co line positions of a transitory blue Doppler shift during the first 1 ns of peak power indicating a speed change of $+200 \pm 100$ and $+500 \pm 100\ \mu\text{m/ns}$ for the pole and film tracers. This is consistent with the measured pole emission trajectory acceleration but may indicate that the film tracer is accelerated through a laser-heated region seen in emission as near stationary. We have examined a number of other model augmentations [29] and find that current hohlraum models are not yet able to account for both the emission trajectory and T_e measurements.

In summary, we have shown for the first time three spatially separated measurements of T_e and plasma flow in a NIF ignition hohlraum using dot spectroscopy. Comparison of the data with models gives evidence of reduced heat transport along the hohlraum axis and classical heat flow at the equator. The tracer trajectories are not reproduced in the simulations and are part of ongoing model investigations.

The authors thank Dr. J. Gaffney for advice on the statistical methods used in the analysis. This work was performed under the auspices of the U.S. Department of Energy by Lawrence Livermore National Laboratory under Contract No. DE-AC52-07NA27344.

*mbarrios@iqt.org

[1] J. Lindl, O. Landen, J. Edwards, E. Moses, and NIC team, Review of the National Ignition Campaign 2009-2012, Phys. Plasmas **21**, 020501 (2014); J. Lindl, O. Landen, J. Edwards, E. Moses, J. Adams, P. A. Amendt, N. Antipa, P. A. Arnold, L. J. Atherton, S. Azevedo *et al.*, Erratum, Phys. Plasmas **21**, 129902 (2014).

[2] O. A. Hurricane *et al.*, Inertially confined fusion plasmas dominated by alpha-particle self-heating, Nat. Phys. **12**, 800 (2016).

[3] J. D. Moody, D. A. Callahan, D. E. Hinkel, P. A. Amendt, K. L. Baker, D. Bradley, P. M. Celliers, E. L. Dewald, L. Divol, T. Dppner *et al.*, Progress in hohlraum physics for the National Ignition Facility, Phys. Plasmas **21**, 056317 (2014).

[4] M. D. Rosen, H. A. Scott, D. E. Hinkel, E. A. Williams, D. A. Callahan, R. P. J. Town, L. Divol, P. A. Michel, W. L. Kruer, L. J. Suter, R. A. London, J. A. Harte, and G. B. Zimmerman, The role of a detailed configuration accounting (DCA) atomic physics package in explaining the energy balance in ignition-scale hohlraums, High Energy Density Phys. **7**, 180 (2011).

[5] A. R. Bell, R. G. Evans, and D. J. Nicholas, Electron Energy Transport in Steep Temperature Gradients in Laser-Produced Plasmas, Phys. Rev. Lett. **46**, 243 (1981).

[6] H. Scott and S. Hansen, Advances in NLTE modeling for integrated simulations, High Energy Density Phys. **6**, 39 (2010).

[7] W. A. Farmer, J. M. Koning, D. J. Strozzi, D. E. Hinkel, L. F. Berzak Hopkins, O. S. Jones, and M. D. Rosen, Simulation of self-generated magnetic fields in an inertial fusion hohlraum environment, Phys. Plasmas **24**, 052703 (2017).

[8] W. A. Farmer, O. S. Jones, M. A. B. Garcia, D. J. Strozzi, J. M. Koning, G. D. Kerbel, D. E. Hinkel, J. D. Moody, L. J. Suter, D. C. Eder, O. L. Landen, D. A. Liedahl, A. S. Moore, and M. B. Schneider, Heat transport modeling of the dot spectroscopy platform on NIF, Plasma Phys. Controlled Fusion **60**, 044009 (2018).

[9] S. H. Glenzer, C. A. Back, L. J. Suter, M. A. Blain, O. L. Landen, J. D. Lindl, B. J. MacGowan, G. F. Stone, R. E. Turner, and B. H. Wilde, Thomson Scattering from

Inertial-Confinement-Fusion Hohlraum Plasmas, Phys. Rev. Lett. **79**, 1277 (1997).

[10] D. H. Froula, J. S. Ross, L. Divol, and S. H. Glenzer, Thomson-scattering techniques to diagnose local electron and ion temperatures, density, and plasma wave amplitudes in laser produced plasmas (invited), Rev. Sci. Instrum. **77**, 10E522 (2006).

[11] C. A. Back, D. H. Kalantar, R. L. Kauffman, R. W. Lee, B. J. MacGowan, D. S. Montgomery, L. V. Powers, T. D. Shepard, G. F. Stone, and L. J. Suter, Measurements of Electron Temperature by Spectroscopy in Hohlraum Targets, Phys. Rev. Lett. **77**, 4350 (1996).

[12] M. A. Barrios, D. A. Liedahl, M. B. Schneider, O. Jones, G. V. Brown, S. P. Regan, K. B. Fournier, A. S. Moore, J. S. Ross, O. Landen, R. L. Kauffman, A. Nikroo, J. Kroll, J. Jaquez, H. Huang, S. B. Hansen, D. A. Callahan, D. E. Hinkel, D. Bradley, and J. D. Moody, Electron temperature measurements inside the ablating plasma of gas-filled hohlraums at the National Ignition Facility, Phys. Plasmas **23**, 056307 (2016).

[13] J. S. Ross, D. H. Froula, A. J. Mackinnon, C. Sorce, N. Meezan, S. H. Glenzer, W. Armstrong, R. Bahr, R. Huff, and K. Thorp, Implementation of imaging Thomson scattering on the Omega Laser, Rev. Sci. Instrum. **77**, 10E520 (2006).

[14] M. Sherlock, J. P. Brodrick, and C. P. Ridgers, A comparison of non-local electron transport models for laser-plasmas relevant to inertial confinement fusion, Phys. Plasmas **24**, 082706 (2017).

[15] S. A. MacLaren, M. B. Schneider, K. Widmann, J. H. Hammer, B. E. Yoxall, J. D. Moody, P. M. Bell, L. R. Benedetti, D. K. Bradley, M. J. Edwards, T. M. Guymer, D. E. Hinkel, W. W. Hsing, M. L. Kervin, N. B. Meezan, A. S. Moore, and J. E. Ralph, Novel Characterization of Capsule X-Ray Drive at the National Ignition Facility, Phys. Rev. Lett. **112**, 105003 (2014).

[16] R. S. Marjoribanks, M. C. Richardson, P. A. Jaanimagi, and R. Epstein, Electron-temperature measurement in laser-produced plasmas by the ratio of isoelectronic line intensities, Phys. Rev. A **46**, R1747 (1992).

[17] T. D. Shepard, C. A. Back, D. H. Kalantar, R. L. Kauffman, C. J. Keane, D. E. Klem, B. F. Lasinski, B. J. MacGowan, L. V. Powers, L. J. Suter, R. E. Turner, B. H. Failor, and W. W. Hsing, Isoelectronic x-ray spectroscopy to determine electron temperatures in long-scale-length inertial-confinement-fusion plasmas, Phys. Rev. E **53**, 5291 (1996).

[18] G. H. Miller, E. I. Moses, and C. R. Wuest, The National Ignition Facility: Enabling fusion ignition for the 21st century, Nucl. Fusion **44**, S228 (2004).

[19] S. B. Hansen, J. Bauche, C. Bauche-Arnoult, and M. F. Gu, Hybrid atomic models for spectroscopic plasma diagnostics, High Energy Density Phys. **3**, 109 (2007).

[20] D. A. Liedahl, M. A. Barrios, G. V. Brown, M. E. Forod, S. B. Hansen, R. F. Heeter, O. Jones, R. Kauffman, O. Landen, C. W. Mauche, J. D. Moody, A. S. Moore, S. P. Regan, J. S. Ross, M. B. Schneider, and K. Widmann, in *Proceedings of the IFSA Conference, Seattle, WA, 2015* (to be published).

[21] F. M. Kerr, A. Gouveia, O. Renner, S. J. Rose, H. A. Scott, and J. S. Wark, Line radiation effects in laboratory and astrophysical plasmas, J. Quant. Spectrosc. Radiat. Transfer **99**, 363 (2006).

[22] D. S. Sivia and J. Skilling, *Data Analysis: A Bayesian Tutorial* (Oxford University Press, Oxford, Great Britain, 2006).

[23] H. Chen, N. Palmer, M. Dayton, A. Carpenter, M. B. Schneider, P. M. Bell, D. K. Bradley, L. D. Claus, L. Fang, T. Hilsabeck, M. Hohenberger, O. S. Jones, J. D. Kilkenny, M. W. Kimmel, G. Robertson, G. Rochau, M. O. Sanchez, J. W. Stahoviak, D. C. Trotter, and J. L. Porter, A high-speed two-frame, 1-2 ns gated X-ray CMOS imager used as a hohlraum diagnostic on the National Ignition Facility (invited), Rev. Sci. Instrum. **87**, 11E203 (2016).

[24] We use 2 μm Fe, 0.76 μm Al, 80 μm of diamond, and 25 μm of Kapton. As a result, 90% of the total Mn emission reaching the detector is from x-ray energies at or above the He-α line at 6.2 keV. In addition, 70% of the total Co emission reaching the detector comes from x-ray energies at or above the He-α line at 7.4 keV.

[25] G. B. Zimmerman and W. L. Kruer, Numerical simulation of laser-initiated fusion, Comments Plasma Phys. Control. Fusion **2**, 51 (1975).

[26] N. Izumi *et al.*, Simultaneous visualization of wall motion, beam propagation, and implosion symmetry on the National Ignition Facility (to be published).

[27] D. W. Forslund, Instabilities associated with heat conduction in the solar wind and their consequences, J. Geophys. Res. **75**, 17 (1970).

[28] M. G. Haines, Magnetic-field generation in laser fusion and hot-electron transport, Can. J. Phys. **64**, 912 (1986).

[29] Changes to the atomic configuration model (modifies the emissivity), finer zoning, and removing the LEH window produce only minor changes in the trajectory. HYDRA [30] and LASNEX emission trajectories [31] are similar. Including 60 J of 30 keV hot electrons beaming onto the dot [32] in the first 1 ns of the laser pulse produces minor changes in the simulated emission trajectory, and including MHD effects increases the hohlraum T_e by 0.3 to 0.5 keV but makes little change to the emission trajectory.

[30] M. M. Marinak, G. D. Kerbel, N. A. Gentile, O. Jones, D. Munro, S. Pollaine, T. R. Dittrich, and S. W. Haan, Three-dimensional HYDRA simulations of National Ignition Facility targets, Phys. Plasmas **8**, 2275 (2001).

[31] O. S. Jones, L. J. Suter, H. A. Scott, M. A. Barrios, W. A. Farmer, S. B. Hansen, D. A. Liedahl, C. W. Mauche, A. S. Moore, M. D. Rosen, J. D. Salmonson, D. J. Strozzi, C. A. Thomas, and D. P. Turnbull, Progress towards a more predictive model for hohlraum radiation drive and symmetry, Phys. Plasmas **24**, 056312 (2017).

[32] E. L. Dewald, F. Hartemann, P. Michel, J. Milovich, M. Hohenberger, A. Pak, O. L. Landen, L. Divol, H. F. Robey, O. A. Hurricane, T. Doppner, F. Albert, B. Bachmann, N. B. Meezan, A. J. MacKinnon, D. Callahan, and M. J. Edwards, Generation and Beaming of Early Hot Electrons onto the Capsule in Laser-Driven Ignition Hohlraums, Phys. Rev. Lett. **116**, 075003 (2016).